Evaluation of Effects of Parameters of Blast Damage Factor, Sub-drilling, Decoupling, and Inter-hole Delay Time on Peak Particle Velocity using Numerical Modeling

Bijan Afrasiabian[1], Kaveh Ahangari[1*], and Ali Noorzad[2]

1. Department of Mining Engineering, Science and Research Branch, Islamic Azad University, Tehran, Iran
2. Department of Civil, Water and Environmental Engineering, Shahid Beheshti University, Tehran, Iran

Abstract

High-level vibrations caused by blasting operations in open-pit mining can exert adverse effects such as destruction of surrounding surface structures. Therefore, it is essential to identify the factors effective in mitigating the damaging effects of ground vibration in open-pit mines, and monitor them. This study investigates the effects of some of the most important blast design parameters in a row of blast holes. According to the advantages of numerical methods, the 3D discrete element method is employed for this purpose. The Peak Particle Velocity (PPV) values are measured along the central hole at the distances of one meter. The results obtained demonstrate that an increase in the blast damage factor and inter-hole delay time results in higher PPV values. However, the increased delay time has no remarkable effect on reducing the development of the blast damage zone. On the other hand, as the decoupling increases, the PPV values diminish, leading to substantial reductions in the ground vibration and rock mass damage. It is also observed that the elimination of sub-drilling does not significantly reduce ground vibrations. The analysis of the results obtained from the numerical modeling show that the discontinuities of the rock mass act as a filter, which could decrease the wave energy by more than 90%. Moreover, it is found that the direction of the discontinuities also affects the emission of waves caused by the blast. The PPV values are reduced, and the damaged zone is less developed if the discontinuities are opposite of the slope surface.

1. Introduction

Today, using explosives for rock fragmentation and extraction is the most economical method, which also has a great safety if proper controls are implemented. In general, almost 20% to 30% of the energy produced during the blasting process (i.e. blast initiation, generation of a shock wave and propagation of blast-induced stress waves in the rock, and high-pressure gas penetration into the rock fractures induced by shock waves) is consumed for fragmentation, and the remaining energy leads to adverse consequences such as ground vibration, air vibration, back-break, and fly-rock [1, 2]. Therefore, the interest in controlling blast-induced vibrations, which are known as the most undesirable effect of blasting operations in open-pit mines and can damage the surrounding

structures, has grown [3]. Several factors generally affect blast-induced vibrations. These factors can be classified as the controllable and uncontrollable parameters [4]. In this regard, 25 parameters were introduced as the effective factors in ground vibration [5].

So far, several researchers have conducted various studies to determine blast-induced vibrations using analytical, empirical, and experimental methods. However, due to the complexity of the blasting procedure, its effects, and the need for accurate prediction of blasting consequences, the analytical and empirical methods do not meet the requirements. These methods have been presented based on the limited datasets of specific case studies, and they cannot be

✉ Corresponding author: kaveh.ahangari@gmail.com (K. Ahangari)

generalized to different conditions. Also the empirical equations are mostly presented for the continuous and homogenous rock masses. Therefore, these equations are not able to consider the effects of discontinuity properties on the blast-induced ground vibrations. In this regard, using the numerical modeling tool was suggested to assess the damages caused by blasting operations [6]. Nowadays, with the development of technology, the advent of robust computers, and the prevalence of numerical methods and related software programs, it has become much easier to model the blasting procedure and predict its effects.

Heretofore, numerous studies have been carried out on the effective parameters in blast-induced vibration. Nevertheless, most of these studies have focused on the parameters of rock mass and discontinuities [7, 8, 9, 10, 11, 12]. A few studies have also been conducted on the effect of different blast design parameters on ground motion caused by the dynamic loading of the blast and damages to the surrounding rock mass and structures. The dynamic response of a jointed phosphorite rock slope to the stress waves caused by blasting using a numerical simulation method was studied [13]. Working on 86 blasting datasets of an open-pit coal mine, the vibrations of blasting was investigated and found that the vibration surfaces strongly depended on the blasting method and type of the used explosive [14]. Vibration records of several blasting in a limestone mine were utilized to present a model capable of estimating the complex waves [15]. The blast-induced damage to a rock mass around a nuclear plant in China using the LS-DYNA and FLAC^{3D} software programs was assessed. It was concluded that the size of the damaged zone increased with an increase in the weight of the explosive [16]. The effects of hole distance from the free face of the bench (burden), blasting initiation location, and placement depth of charge on bench blasting was evaluated using the AUTODYN software [17]. Some parametric studies were conducted on the factors such as loading density, rock mass index (RMR), and the explosive weight to predict the damage caused by blasting using the LS-DAYNA finite element software [18]. The parameters spacing of blast holes and blast loading in the pre-split method has been studied using the 2D discrete element method [19]. In the recent studies, detonation of a row of blast holes using the 3D discrete element code (3DEC) was modeled to evaluate the effects of some rock mass and blast design parameters including rock mass quality, burden and spacing, blast hole diameter, stemming length, and air-

decking on ground vibration [20, 21]. The bench health under the explosive loading in the Hoek-Brown failure criterion using the finite difference method was evaluated. It was resulted that using different parameters of the rock mass in the blast-induced damage zone behind the hole resulted in thoroughly different PPV values that were different from the constant parameters [22].

This paper focuses on the ground vibration induced by the explosion of a row of blast holes to determine the blast-induced damage zone based on the PPV values recorded in monitoring points. In this regard, the response of a rock slope to the ground vibration caused by variation of chosen parameters of blast design has been investigated. According to the advantages of numerical methods over other ones, the 3D discrete element code of 3DEC (version 5.20), in which the rock blocks could have a linear or elastoplastic behavior, was employed to examine the effects of the chosen parameters on the blast wave transmission. Although many studies have been conducted to control the damage zone caused by ground vibrations and blast waves, none have been able to provide an approach that could predict the damage zone caused by ground vibrations.

The main aim of this paper is to provide a practical guideline for mining engineers to predict blast-induced ground vibrations. In addition, the used approach can help the engineers to find solutions to prevent adverse consequences of blasting considering the blast design parameters, and the geological discontinuities from the blast source. In this regard, the ground vibrations and rock mass damages could be controlled by changing the blast design parameters according to allowable ranges.

2. Materials and methods
2.1. Numerical model geometry

In this study, two typical well-accepted geometry of the mining rock slope with 55° benches face angle was considered. Therefore, the dimensions of the numerical model were chosen in such a way that the effects of the explosion up to full attenuation (safe zone) could be perfectly represented. In the initial model of this study, two rock slopes were created with three benches with the dimensions (150 m × 50 m × 80 m) in the X, Y, and Z coordinates. The height of each one of the benches was defined as 15 m. In the models, three discontinuities were considered with two modes of the direction of discontinuities and a spacing of 15 m. In the first mode, they were along the direction

of the slope surface, while in the second one, they were in the opposite direction of the slope surface. The dip of the discontinuities was assumed to be 45° relative to the horizon. The distance between the first discontinuity and the position of the blast holes was 10 m. The numerical model geometry is shown in Figure 1. The blast holes were defined with a diameter of 200 mm and a length of 15 m,

equal to the bench height. Table 1 presents the blast design parameters of the blast holes (in a row) of the initial model. Each parameter in the numerical model was increased within its allowable range to conduct a parametric study on the blast vibrations. A flowchart numerical steps modeling is presented in Figure 2.
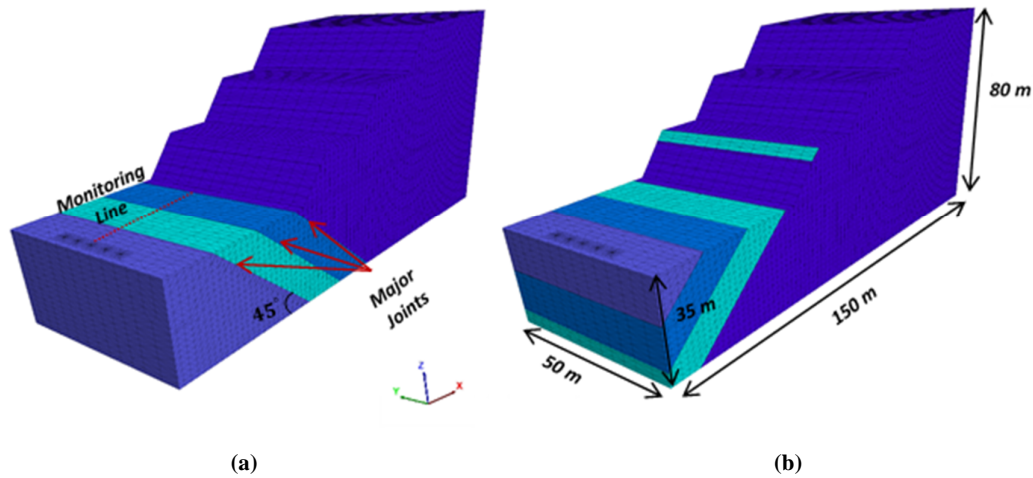

(a)   (b)
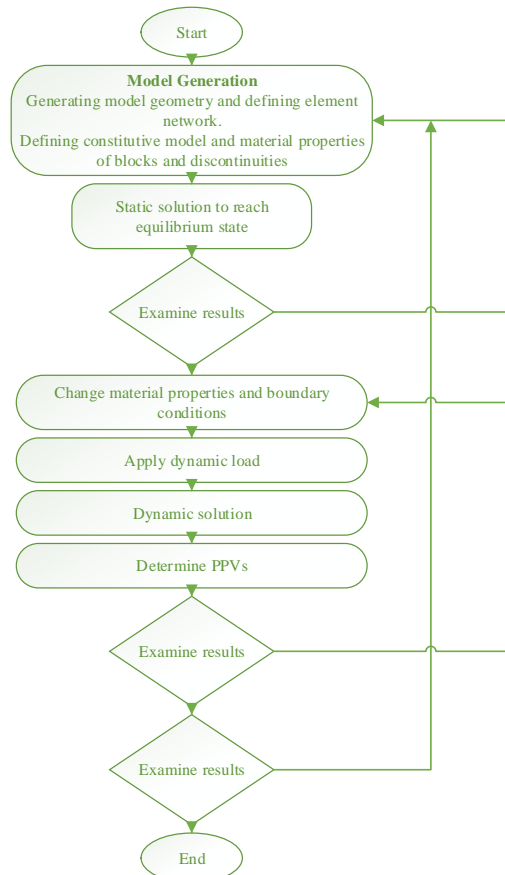
Figure 1. Geometry of rock slopes.

Figure 2. Flowchart of numerical steps.

Table 1. Blast design parameters of the numerical model.

Parameter	Value	Unit
Charge weight	347.1	Kg
Blast hole diameter	200	mm
Burden	4	m
Blast holes spacing	5	m
Stemming length	2.3	m
Sub-drilling length	1.2-2	m

2.2. Determination of mesh dimensions

The meshes in the form of pyramidal tetrahedrons were applied in the present numerical model. The dimensions of meshes should be chosen within (0.1-0.125) of the smallest wavelength of the largest frequency [23, 24]. Therefore, dimensions of the mesh elements were considered 4 m. Given the importance of the areas around the blast holes, the dimensions of the mesh elements were defined much smaller (10 cm), increasing with the distance from the blast holes edges to a radius of 2.5 m with a coefficient of 1/2.

2.3. Determination of constitutive model and material properties of blocks and joints

The suggested values for the intact rocks of granite and diorite were used as the strength properties of the model blocks in the study [25]. The Rocklab software (*version 1.010*) was used to determine the parameters of the rock mass. According to the rock mass conditions, the Hoek–Brown failure criterion was considered for the studied area (Equations 1-4) [26]. This failure criterion is the most suitable one for rock masses with a ductile (elastic-perfectly plastic) behavior or those showing a strain weakening behavior (post-yield strength reduction) [27]. On the other hand, the Coulomb-Slip constitutive model was considered for the discontinuities of the numerical models. This constitutive model is an area contact model, in which the deformations and displacements of discontinuities in the normal and shear directions are affected by its normal and shear stiffnesses. The properties of the block materials and the discontinuities for the high-strength (granite) and medium-strength (diorite) rocks are presented in Table 2.

$$\sigma_1 = \sigma_3 + \sigma_{ci}(m_b\,\sigma_3/\sigma_{ci} + s)^a \tag{1}$$

where σ_1 and σ_3 are the major and minor principal stresses (MPa), respectively, σ_{ci} is the unconfined compressive strength of the intact rock (MPa), and m_b is the reduced value of the materials constant for the intact rock, m_i, obtained from Equation (2).

$$m_b = m_i\,exp(GSI - 100/28 - 14D) \tag{2}$$

where m_i is the curve fitting parameter obtained from triaxial tests on the intact rock, *GSI* is the Geological Strength Index, and *D* is the dimensionless blast damage factor, which depends on the degree of disturbance created in the rock mass by the blast load.

s and *a* are also dimensionless empirical constants, which can be calculated by Equations (3 and 4), respectively.

$$s = exp(GSI - 100/9 - 3D) \tag{3}$$

$$a = 1/2 + 1/6\left(e^{-GSI/15} - e^{-20/3}\right) \tag{4}$$

Table 2. Properties of block materials and discontinuities [21].

Mechanical properties	Diorite value	Granite value	Unit
Density (ρ)	2.5	2.7	(g/cm^3)
Uniaxial compressive strength (*UCS*)	80	150	(MPa)
Bulk modulus (*K*)	4.5	28.9	(GPa)
Shear modulus (*G*)	2.7	21.7	(GPa)
Block cohesion strength (*C*)	1.1	4.1	(MPa)
Joint normal stiffness (JK_n)	0.5	0.5	(GPa/m)
Joint shear stiffness (JK_s)	0.25	0.25	(GPa/m)
Joint friction angle (φ_j)	30	30	(°)
Joint cohesion (C_j)	15	15	(MPa)

2.4. Static solution

The boundary conditions should be defined prior to the development of the static solution [28]. In this regard, the boundaries of the two sides (left and right) and the bottom of the model were assumed to be fixed to present the real-space effects. However, the front and top sides of the model were considered free faces. In Figure 3a, the static boundary condition is shown. Afterward, the initial

equilibrium of the rock slope was assessed to properly distribute the stress in the model and create real conditions. Therefore, the model equilibrium was ensured by evaluating the unbalancing forces, as well as the history of displacements in different points on the model surface. After drilling of the blast holes, the model was statically solved again to reach the equilibrium.
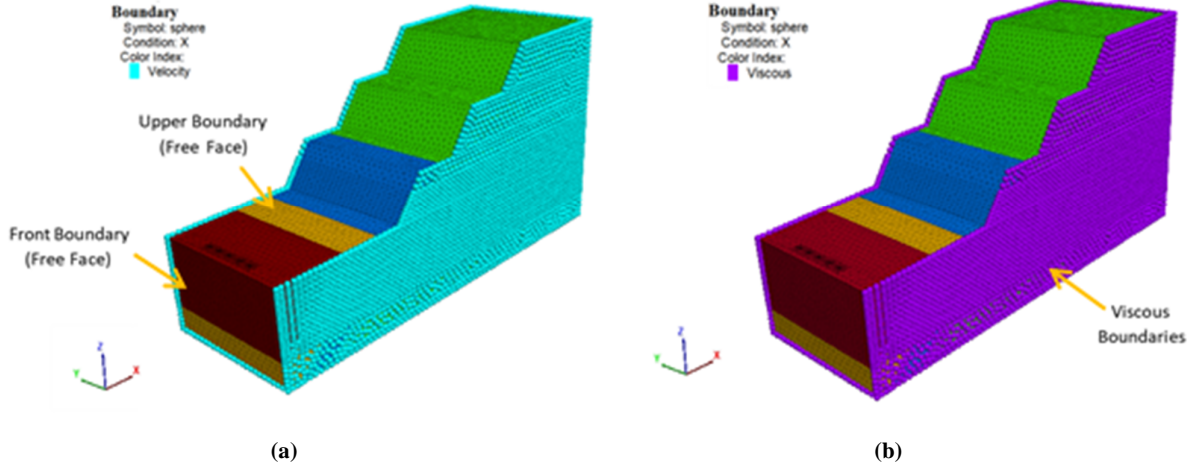

(a)   **(b)**

Figure 3. Boundary conditions (a) Static state boundary (b) Dynamic state boundary.

2.5. Dynamic borehole pressure

The pressure produced by the explosives in the blast hole can be considered as the main parameter of blasting. Concerning the blast-induced pressure, blast damage zone is determined by comparing the rock mass strength against compressive or tangential stresses produced by an explosive charge. Various empirical relationships have been proposed by the researchers for dynamic loading caused by blasting so far [29, 30, 31, 32]. The pressure-decay function, which was presented based on the Starfield and Duvall's relationship, was used in this research work to apply the pressure produced by the dynamic impact process caused by the blasting of ANFO (ammonium nitrate and fuel oil) explosive to the hole wall (Equations 5-8) [19]. This function has two advantages over the other ones. First, it simulates borehole pressure caused by the blasting of ANFO, which is a non-ideal explosive, more accurately [33]. Secondly, unlike other functions, it takes the properties of rock mass and explosive into account. In this regard, the function of pressure-decay resulting from the blasting of ANFO was coded using the FISH programming language in the 3DEC software and applied to the walls and bottom of the blast holes in the form of compressive stress. This dynamic loading function was in the form of a pressure-time pulse applied as stress history to the walls of the blast holes (Figure 4).

$$PD = 432 \times 10^{-6}(\rho_e VD^2/1 + 0.8\rho_e) \tag{6}$$

$$PE = PD/2 \tag{7}$$

$$PW = PE(r_h/b)^{-qk} \tag{8}$$

where *PD*, *VD*, *PE*, and *PW* denote the detonation pressure (MPa), detonation velocity (m/s), the pressure of gases produced by blasting (MPa), and borehole pressure in the complete coupling of explosive and blast hole wall (when there is no gap between the blast hole wall and the explosive), respectively. Moreover, r_h, *b*, *k*, and *q* are the blast hole radius (mm), explosive radius (mm), specific heat capacity, and explosive shape factor (2 for cylindrical charges and 3 for spherical charges), respectively [34, 35].

It is worth noting that according to the Starfield's relationships, the dynamic borehole pressure produced by blasting is a function of time and depends on factors such as rock density (ρ_r), explosive density (ρ_e), longitudinal wave velocity (C_p), and velocity of detonation (*VD*). Accordingly, the dynamic borehole pressure caused by blasting can be calculated using Equation (8).

$$P(t) = PW \cdot (8\rho_r \cdot C_p / \rho_r C_p + VD \cdot \rho_e) \left[e^{(-Bt/\sqrt{2})} - e^{-\sqrt{2Bt}} \right]$$

(8)

$$B = 16338$$

where *P(t)* is the borehole pressure history (MPa), C_p is the longitudinal wave velocity (m/s), and t is the time (s).

Since the relationship depends on the rock density, explosive density, and longitudinal wave velocity, different borehole pressures of the chosen rocks were considered based on the properties of the rock mass and the explosive (Figure 4). Due to the limitations of the 3DEC software in the direct application of normal force to a plane, the dynamic loading caused by the blasting was considered as a compressive stress history and applied hydrostatically to the blast holes walls and bottom. The compressive blasting stress was selected based on the lengths of the explosive charge to satisfy the charge length of each hole, as well as the level of load applied to it. The parameters used for the ANFO explosive in Starfield and Duvall's relationship are presented in Table 3.
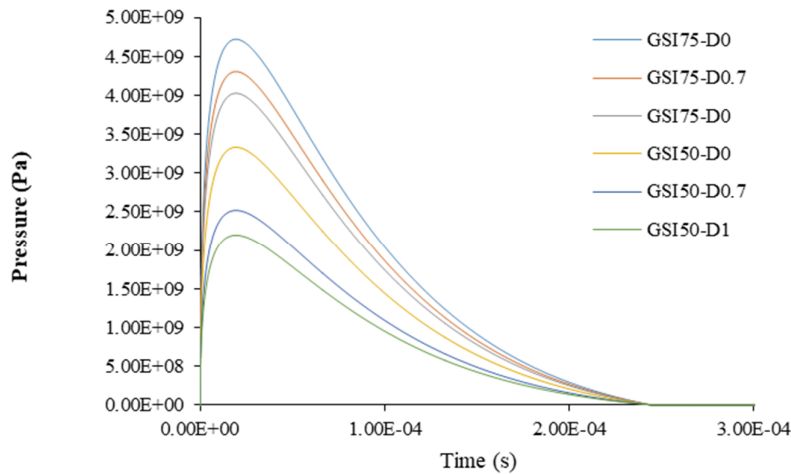

Figure 4. History of borehole pressure caused by blasting of ANFO.

Table 3. Used parameters for the ANFO explosive in Starfield and Duvall equation [32].

Parameter	Value	Unit
Velocity of detonation (VOD)	4500	(m/s)
Explosive density (ρ_e)	0.850	(g/cm³)
P-wave velocity (C_p)	4625	(m/s)
Specific heat coefficient (k)	1.2	---
Explosive shape factor (q)	2	---

2.6. Determination of dynamic boundary conditions and damping

Generally, in dynamic analyses, the waves produced by dynamic energy can be reflected in the model. Therefore, the dynamic waves should become damped to avoid the effects exerted by their reflection [23]. Consequently, viscous (non-reflecting) boundaries were used for the lateral and bottom sides of the model (Figure 3b). The local damping of 5% was used in the modeling, as suggested by the previous studies [36]. Afterward, the models were solved dynamically, and the PPV values were recorded and updated continuously. This process continued until the PPV values got included within the allowable range or approached to zero.

2.7. PPV measurement

Ground vibration can be measured based on velocity, displacement, acceleration, and frequency. Among the mentioned parameters, PPV has been well accepted as the most proper one to determine the direction of blast-induced ground vibration [37]. Equation (9) illustrates the general form of this parameter [38].

$$PPV = KSD^{-b} \qquad (9)$$

where *PPV* is the peak particle velocity (mm/s), *SD* is the scaled distance (m/kg$^{1/2}$) calculated by (R/Q$^{1/2}$), and *K* and *b* are the constants associated with the site.

To determine the PPV values, Equation (10) was proposed [39]. According to Equation (10), the PPV values can be calculated using the components of wave velocity in three perpendicular directions (longitudinal, transverse, and vertical) [39]. In fact, the level of created vibrations is obtained from the maximum unit value of velocity components or the sum of squares of real vectors of the three components' maximum values. This relationship was coded using the FISH programming language in the 3DEC software, and its values were calculated in the monitoring points.

$$PPV = \sqrt{(V_{max})_x^2 + (V_{max})_y^2 + (V_{max})_z^2} \qquad (10)$$

where *PPV* is the peak particle velocity (mm/s), and V_x, V_y, and V_z are the velocity components in longitudinal, transverse, and vertical directions (m/s), respectively.

The peak particle velocities were recorded in both near-field blasting region (i.e. immediate area surrounding the blast hole) and far-field blasting region (i.e. the area that intensity of the generated blast-induced waves diminishes to a level where no permanent deformation is caused) [33]. In this regard, the PPVs were measured, along the X-axis from the central hole collar to the end of the model. It should be pointed out that the spacing of the monitoring points was considered as a proportion of the mesh dimensions.

3. Results and discussion

The blasting process has a complex nature. This means that the blasting performance depends on various parameters. Blasting is considered as the most effective factor of disturbance in rock slopes. In order to determine the blast-induced damages, using numerical methods were suggested [40]. The most important effective parameters in ground vibration were introduced in the previous studies [41, 30]. These parameters generally include the ones associated with the properties of rock mass and the blast design parameters. Therefore, the blast design parameters and blast damage factor (of Hoek–Brown criterion) and their effects on ground vibration were investigated in this section of the study. It should be noted that all of the modelings were conducted to evaluate the mentioned parameters in a rock slope in the presence of discontinuities, and the results were presented accordingly.

3.1. Effect of blast damage factor on PPV values

The parameter D as disturbance (blast damage) factor was introduced to improve the prediction accuracy of rock mass strength against the blasting conditions [26]. Considering the damage caused by mechanical excavation and production blasting, the values of 0 for an undisturbed rock mass and 1 for a severely disturbed was suggested [26]. In this research work, three values of 0, 0.7, and 1 were considered for the blast damage factor to assess its effect on the PPV values and ground vibrations. The values of PPV for the granite and diorite in two directions of discontinuities are presented in Figures 5 and 6.
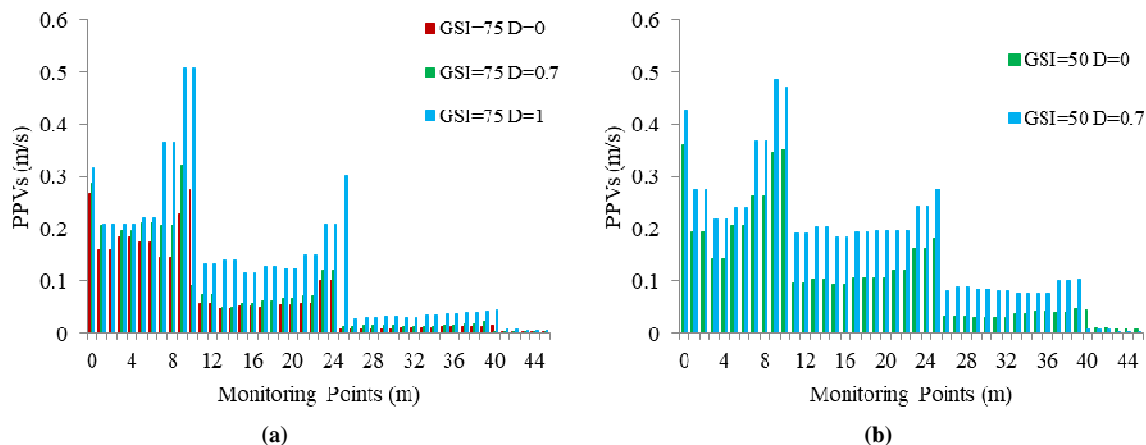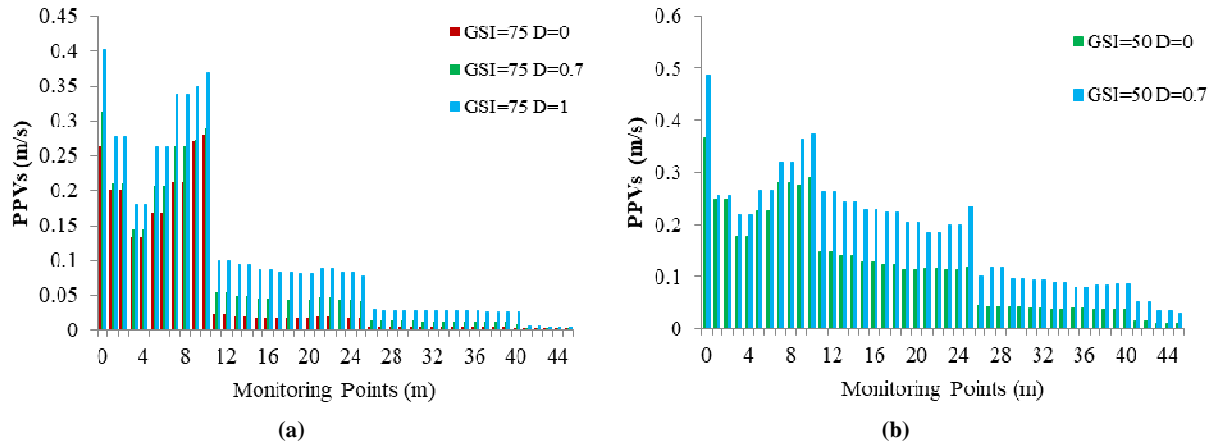

(a)   **(b)**

Figure 5. PPVs with different damage factors and the first mode of discontinuities a) granite, b) diorite.

Figure 6. PPVs with different damage factors and the second mode of discontinuities a) granite, b) diorite.

As shown in Figures 5 and 6, the waves caused by the blasting of the charge column had a descending trend, and the PPV values decreased with an increase in the distance from the blasting location. Since geological discontinuities are naturally the weakest part of a rock mass, the PPV values in these points increased locally. With a reduction in the rock mass strength caused by the increase in the blast damage factor (D), the PPV values in the monitoring points increased. Furthermore, the results obtained from the numerical modelings illustrated that the presence of discontinuities could degrade a part of the incident wave energy. Meanwhile, a part of the wave energy passes through the discontinuity and another part is reflected. As shown in Figures 5 and 6, the degradation of the blast wave energy in the granite (UCS = 150 MPa) was more than that in the diorite (UCS = 80 MPa). According to Figure (5a), in the first mode of the direction of discontinuities (along to the direction of the slope surface) for (GSI = 75, D = 0), PPV after the collision of the blast wave with the first discontinuity was 134 mm/s. However, by increasing the blast damage factor to 0.7 and 1, the PPV values increased to 323.2 mm/s and 509.5 mm/s. The second mode of the direction of discontinuities (opposite of the slope surface) in Figure (6a) follows a similar trend. In this mode, the PPV values recorded in the monitoring points also increased with an increase in the blast damage factor, with the values of 279.94 mm/s, 288.92 mm/s, and 368.74 mm/s recorded for D = 0.7, D = 0, and D = 1,

respectively. It is worth mentioning that although a similar trend of reduction in the PPV values with the increase in the blast damage factor was observed in both modes of discontinuities, for the discontinuities with a direction opposite of the slope surface, the recorded PPV values were lower than those in the first mode.

A similar trend is also observed for the diorite in Figures (5b) and (6b). Accordingly, in the first mode of discontinuities, the PPV values increased from 353.31 mm/s to 473.12 mm/s by increasing the blast damage factor from 0 to 0.7, while in the second mode, the PPV values of 289.74 mm/s and 364.15 mm/s were recorded, respectively.
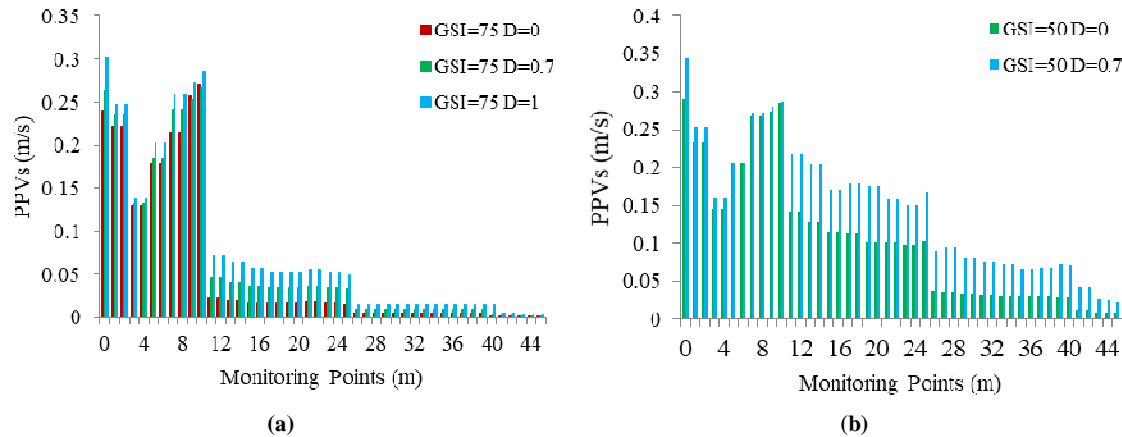
3.2. Effect of the sub-drilling length on PPV values

In the open-pit mines blasting operations, blast holes are often drilled from the top of the benches to a little below the desired floor level. The reason for drilling in such a way is to make the maximum stress area closer to the bench floor and prevent the formation of a toe at the bottom of the bench. Ash suggested (*0.2B-0.5B*) for the sub-drilling length in vertical holes depending on the rock mass strength [42]. According to the allowable range for granite and diorite, the sub-drilling length in the blast holes was considered 1.2 m and 0.8 m, respectively, and the obtained results were compared with those of the case without sub-drilling. Figures 7 and 8 indicate the effect of this parameter on the PPV values.
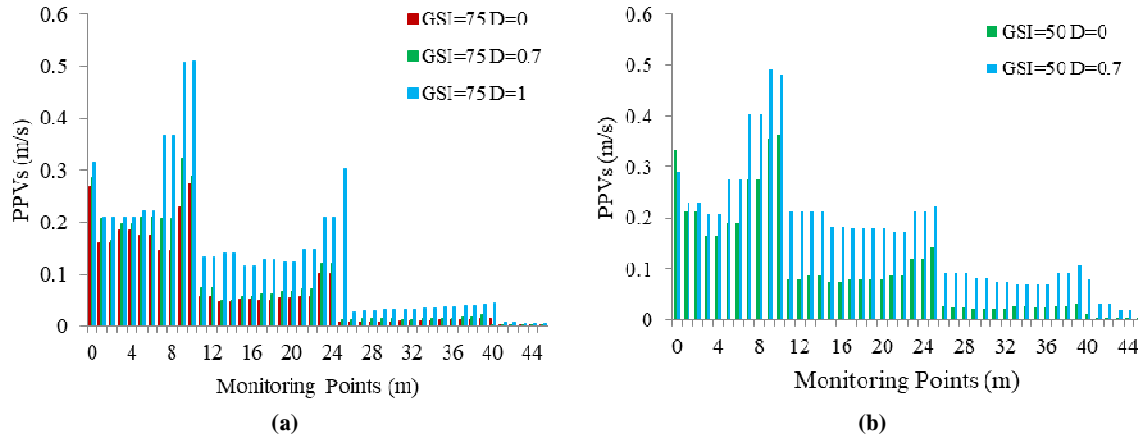
Figure 7. PPV values with the elimination of sub-drilling and the first mode of discontinuities a) granite, b) diorite.

Figure 8. PPV values with the elimination of sub-drilling and the second mode of discontinuities a) granite, b) diorite.

These figures also show the effect of sub-drilling length in the two modes of the direction of discontinuities for the granite and diorite with different values of blast damage factor (0, 0.7, and 1). By comparing the results obtained from the modelings with (Figures 5 and 6) and without sub-drilling (Figures 7 and 8), it was found that the elimination of sub-drilling led to lower PPV values. The reduction in the PPV values was due to the reduced length of loading caused by blasting, as well as the lower consumed specific charge.

Excessive sub-drilling can increase vibration because of the lack of a nearby free face to create reflection waves [8]. Although the sub-drilling increases explosive consumption, the standard length of the sub-drilling did not a significant effect on the ground vibrations. The obtained results of the numerical models have shown that the sub-drilling does not have a crucial effect on reducing the ground vibration levels. This is due to the lack

of stress wave energy to move to the ground surface.

3.3. Effect of decoupling on PPV values

Generally, decoupling is referred to as conditions in which the explosive does not completely fill the blast hole diameter [33]. In the decoupled area, which is located in the radial range of ($r_e \leq r \leq r_h$), the void space between the explosive charge and the borehole wall is usually filled with water or air [43]. The decoupling ratio increases with an increase in the hole radius or a decrease in the explosive radius. Various studies have investigated the effect of decoupling so far. However, most of them have focused on the fragmentation performance of rock mass under dynamic loading of blasting, and only a few researchers have assessed the effect of this parameter on ground vibration. Previous studies stated that complete

coupling of a charge column creates more ground vibrations [44]. The effect of decoupling on ground vibration at three (r_e/r_h) ratios of 0, 1/2, and 2/3 was studied in this research work. The PPV values obtained for granite and diorite are shown in Figures 9 and 10.
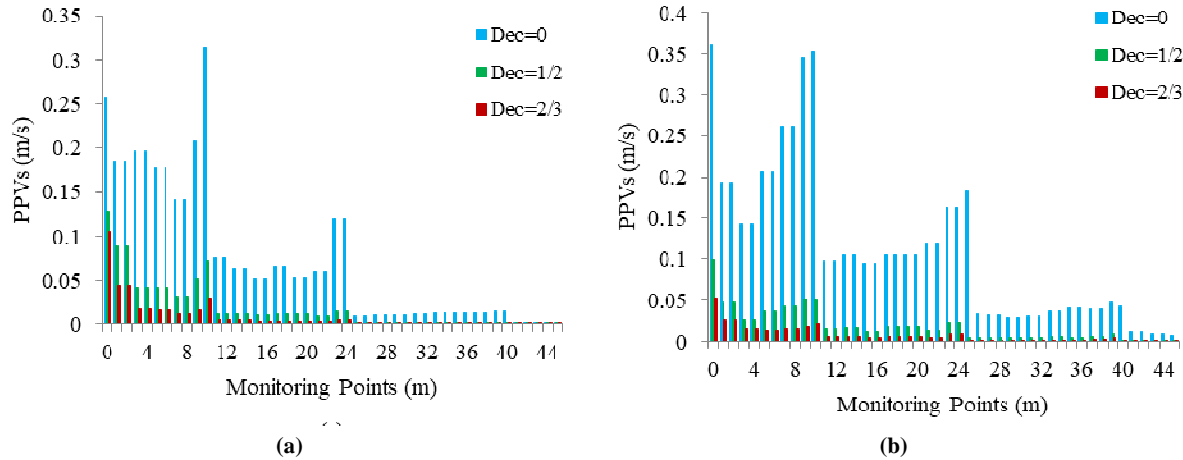

Figure 9. PPV values for different values of decoupling and the first mode of discontinuities a) granite, b) diorite.
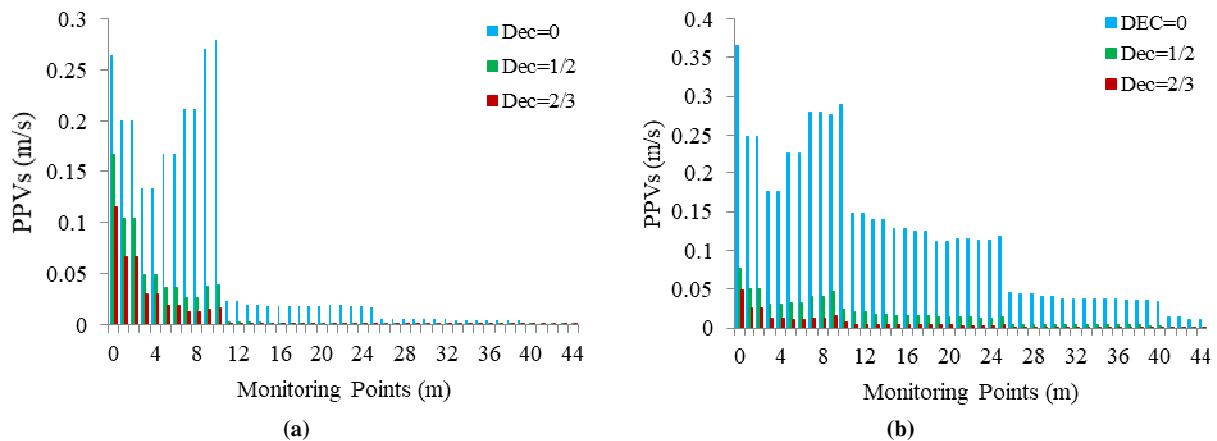

Figure 10. PPV values for different values of decoupling and the second mode of discontinuities a) granite, b) diorite.

As shown in the figures, the PPV values recorded in the monitoring points were higher when the diameters of the explosive and blast hole were equal, and the explosive had complete contact with the blast hole wall (complete coupling). This can be attributed to the increases in the specific charge, and consequently, the dynamic load caused by the blasting of the explosive on the blast hole wall. Meanwhile, in all models, the PPVs were diminished by the rise of the decoupling. According to the results shown in Figure (9a), as the coupling was reduced by 50% and 66.6%, the PPV values recorded in the first discontinuity (at a distance of 10 m from the blast hole) decreased by 77.2% and 90.2%, respectively. The reduction of PPV values for the diorite was also 85.7% and 94.2%, respectively.

On the other hand, in the second mode of the discontinuities, the reduction of coupling by 50% and 66.6% in the granite lowered the PPV values at the first discontinuity by 86% and 94%, respectively. The corresponding reductions of PPV values for the diorite were 92.9% and 97.9%, respectively. As mentioned, the results obtained from the numerical modelings revealed that the use of the decoupling technique could significantly reduce the blast-induced ground vibrations. Therefore, this technique can be proposed and used as an efficient option along with other methods in controlled blastings or those close to sensitive centers or residential buildings.

3.4. Effect of delay time of blast holes on PPV values

Using delay time in blasting operations allows for the blasting charges to blast at defined time intervals between them. It is possible to control the quality of rock mass fracture and the movement direction of rocks in this method [33]. Delay time and geometry of blast holes can affect blast-induced ground vibrations [33]. In the present study, two different patterns were investigated for the blasting of the holes as follows (Figure 11): 1) linear blasting pattern (sequential blasting of holes), 2) non-linear blasting pattern (start of blasting from the central hole).
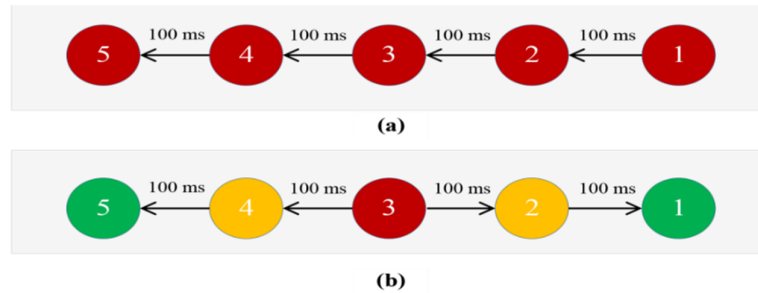

Figure 11. Blasting patterns: a) linear, b) non-linear.

In the linear blasting pattern, the detonations of holes occurred (with a definite delay time) from the first to the last one. On the other hand, in the non-linear blasting pattern, the central hole (blast hole No. 3) detonated at first, followed by the delayed blasting of the surrounding holes. Accordingly, three lengths of delay time (0, 50, and 100 ms) were modeled to assess the effect of blast delay time on PPV values. The obtained PPVs for these delay time in both granite (GSI = 75, D = 0) and diorite (GSI = 50, D = 0) are illustrated in Figures 12 and 13.
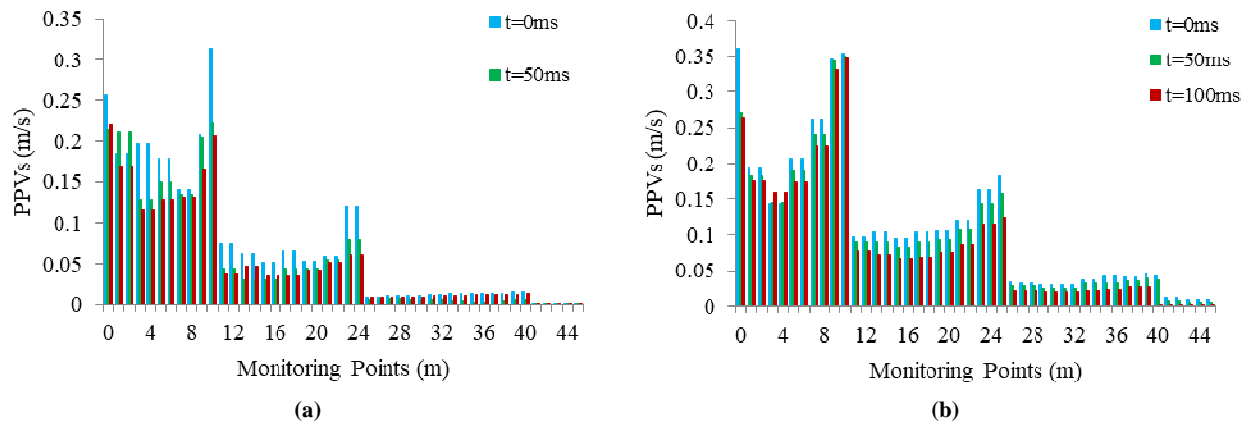

Figure 12. PPV values for different delay time with the linear blasting pattern and the first mode of discontinuities a) granite, b) diorite.

As it can be seen in the figure, the increase in the delay time resulted in reduced PPV values in the monitoring points. In fact, the delay time between detonations of the holes produced separate wave fronts associated with different charges. Therefore, this process eliminated the superposition effects of the waves and reduced the PPV values recorded in the monitoring points. It should be noted that in the linear blasting pattern, the PPV values showed smaller changes with the increase in the blast delay time when the direction of the geological discontinuities was along to that of the rock slope surface. As shown in Figure (12a), by increasing the delay time from 0 ms (simultaneous blasting) to 50 ms and 100 ms for the granite, the PPV values decreased from 314.25 mm/s to 221.84 mm/s (29.40% reduction) and 206.50 mm/s (34.28% reduction), respectively. Moreover, according to Figure (12b), the similar changes in the blast delay time lowered the PPV values from 353.32 mm/s to 350.14 mm/s (about 1% reduction) and 347.20 mm/s (about 1.8% reduction), respectively. It is worth mentioning that the reported values solely belong to the monitoring point on the first

discontinuity and the reduction in PPV values could vary in different monitoring points due to the complex nature of the geological conditions.

As shown in Figure 13, by changing the direction of the discontinuities (to the opposite of the slope surface), like the former mode, the obtained results indicated a decreasing trend for both diorite and granite. A comparison of Figures 12 and 13 reveals that when the discontinuities were opposite of the slope surface, the PPV values in the monitoring point (on the first discontinuity) decreased with a

higher rate than that of the former mode. According to Figure (13a), the PPV values reduced by 48.27% and 66.42%, respectively, as the delay time increased from 0 ms (simultaneous blasting) to 50 ms and 100 ms. This decreasing trend was also observed for the diorite (Figure 13b). With the similar rises in the blast delay time for this rock with the second mode of discontinuities, the PPV values decreased by 16.2% and 31.3%, respectively.

(a)   **(b)**

Figure 13. PPV values for different delay time with the linear blasting pattern and the second mode of discontinuities a) granite, b) diorite.
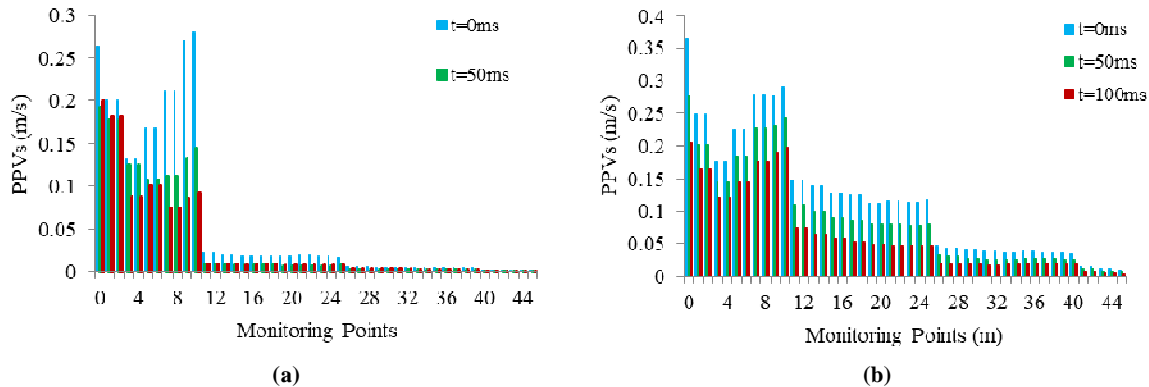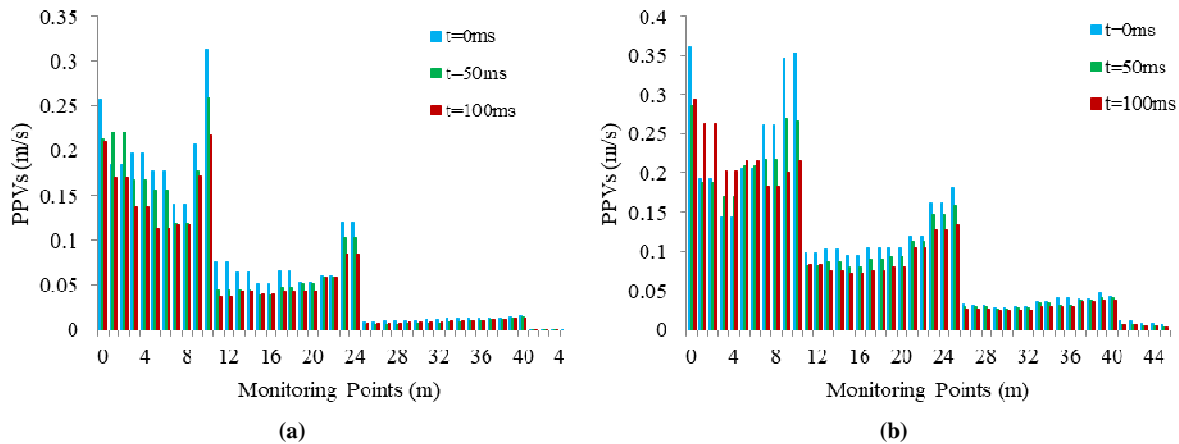

(a)   **(b)**

Figure 14. PPV values for different lengths of delay time with the nonlinear blasting pattern and the first mode of discontinuities a) granite, b) diorite.

According to Figures 14 and 15, in the non-linear blasting pattern, the decreasing trend of PPV values was observed for both modes of discontinuities in the granite and diorite rock masses with the increase in the blast delay time in two steps (50 ms and 100 ms). The results obtained from the numerical modelings for the non-linear blasting pattern showed some dispersions in the PPV values recorded in the areas around the blast

hole. Therefore, it seems that in these areas, the PPV values did not follow a particular trend with the rise in the delay time. However, after a collision with the first discontinuity, the PPV values reflected a decreasing trend similar to that of the linear pattern. Although the overall trend of PPV values in the monitoring points was decreasing in the non-linear blast pattern, it did not follow a specific trend in the areas around the blast hole.
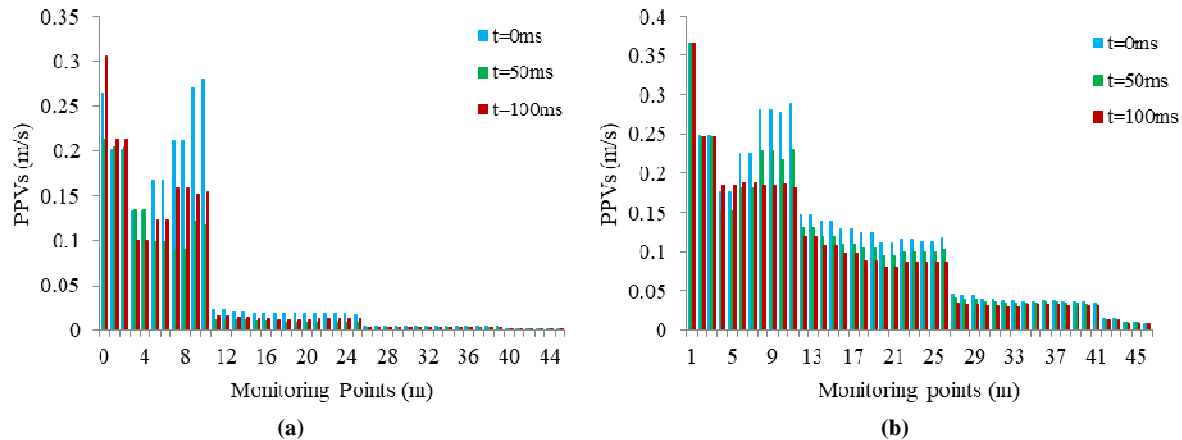
Figure 15. PPV values for different lengths of delay time with the nonlinear blasting pattern and the second mode of discontinuities a) granite, b) diorite.

4. Blast-induced Damage Criterion

So far, many researchers have considered PPV as the most appropriate parameter to determine the ground vibration since it can be easily measured [45, 46, 47]. In the case when PPV is considered as a damage index, the damage zone is defined as the distance between the blast hole and a point of the rock mass, where the PPV values cannot break it [48]. The researchers have suggested various values for blast-induced damage threshold [49, 50, 51]. In this research work, the damage zone was determined based on the standard of Bhandari *et al.* after the measurement of the PPV values. The 50 mm/s as the rock mass damage threshold was considered [20]. After the blasting, the PPV values were monitored and recorded at the distances of 1 m from the central hole to the rock slope edge.

4.1. Determination of blast damage areas based on threshold PPV values

To more precisely assess the effects of each chosen parameter and determine the blast damage zone, the maximum PPV values were recorded at four monitoring points at the distances of 0, 10, 25, and 40 m (including the blast hole collar and discontinuity surfaces). Bhandari considered the PPV of 50 mm/s as the damage threshold in rock conditions. Accordingly, the values recorded in the monitoring points were divided into two groups. The first group, shown in blue color, indicated the safe zone of the rock mass (PPV < 50 mm/s). On the other hand, the second group, shown in red color, indicated the blast damage zone, where the rock mass was completely damaged (PPV ≥ 50 mm/s) (Tables 4-13).

Table 4. Maximum PPV values on the blast hole collar and the first mode of discontinuities.

Distance from the blast hole (m)	PPV(mm/s)				
	GSI = 75, D = 0	GSI = 75, D = 0.7	GSI = 75, D = 1	GSI = 50, D = 0	GSI = 50, D = 0.7
0	267.96	287.08	317.30	361.16	426.83
10	273.93	323.28	509.56	353.31	485.94
25	100.20	118.82	302.09	182.08	275.49
40	15.49	22.62	42.80	46.43	104.02

Table 5. Maximum PPV values on the blast hole collar and the second mode of discontinuities.

Distance from the blast hole (m)	PPV(mm/s)				
	GSI = 75, D = 0	GSI = 75, D = 0.7	GSI = 75, D = 1	GSI = 50, D = 0	GSI = 50, D = 0.7
0	264.29	311.67	401.29	365.78	487.40
10	279.74	288.92	368.74	289.74	372.08
25	17.93	43.48	77.19	117.88	235.08
40	4.71	12.56	26.05	35.82	87.84

As shown in Tables 4 and 5, the PPV values were measured and recorded in both directions of discontinuities for both granite (GSI = 75) and diorite (GSI = 50) rock masses with different blast

damage factors. Comparison of the results obtained from the numerical modelings demonstrated that in both directions of the discontinuities, the increase in the blast damage factor (D) resulted in higher PPV values in the monitoring points, and consequently, a more damaged rock mass. It was also found that the damages of the granite rock mass were less in the second mode of discontinuities. It was revealed that the damage to the rock mass in the models (GSI = 75, D = 0.7) and (GSI = 75, D = 0) extended 10 m from the blast hole (the location of the first discontinuity). Meanwhile, in the models (GSI = 75, D = 1) and (GSI = 50, D = 0), the damaged area developed 25 m from the blast hole (the location of the second discontinuity). On the other hand, a comparison of Tables 4 and 5 showed that for the first mode of the

direction of discontinuities, the blast-induced damage to the rock mass developed more in the models (GSI = 75, D = 0.7) and (GSI = 75, D = 0) and extended to the location of the second discontinuity. This can be attributed to the reflection and superposition of the waves after collision with the discontinuity surface and transmission of a portion of it to the surface. Furthermore, in the model (GSI = 50, D = 0.7) for both modes of the direction of discontinuities, the diorite rock mass sustained the highest damage, which extended to the location of the third discontinuity. This is due to 1) its lower uniaxial compressive strength compared to the granite rock mass and 2) the increase in the blast damage factor (D = 0.7).

Table 6. Maximum PPV values on the blast hole collar and the first mode of discontinuities with the elimination of sub-drilling.

Distance from the blast hole (m)	PPV(mm/s)				
	GSI = 75, D = 0	GSI = 75, D = 0.7	GSI = 75, D = 1	GSI = 50, D = 0	GSI = 50, D = 0.7
0	270.24	267.02	272.14	332.01	290.73
10	316.62	249.43	463.19	362.93	490.55
25	57.00	68.30	92.71	141.71	220.53
40	7.17	13.53	11.16	29.90	106.45

Table 7. Maximum PPV values on the blast hole collar and the second mode of discontinuities with the elimination of sub-drilling.

Distance from the blast hole (m)	PPV(mm/s)				
	GSI = 75, D = 0	GSI = 75, D = 0.7	GSI = 75, D = 1	GSI = 50, D = 0	GSI = 50, D = 0.7
0	240.00	263.60	301.33	290.31	344.62
10	270.99	267.23	285.67	285.31	287.68
25	15.92	34.13	43.80	102.81	167.80
40	0.63	8.96	14.49	28.90	71.15

As shown in Tables 6 and 7, the results illustrated that the elimination of sub-drilling had no considerable effect on reducing the development of the damage zone, and only led to a slight reduction of PPV values in some monitoring points. In the second mode of discontinuities, it can be concluded that by eliminating the sub-drilling the PPVs reduced under the damage threshold only in the

model (GSI = 75, D = 1). It means that the safe zone developed to 25 m from the blast hole collar. Regardless of the marginal effect of this parameter on reducing the damage zone, applying it to blast designs allows for better distribution of energy at the bottom of the blast hole, which can bring down the costs caused by secondary blasting.

Table 8. Maximum PPV values on the blast hole collar and the first mode of discontinuities with different values of decoupling.

Distance from the blast hole (m)	PPV(mm/s)			
	GSI = 75, D = 0		GSI = 50, D = 0	
	DEC = 1/2	DEC = 2/3	DEC = 1/2	DEC = 2/3
0	165.85	114.92	76.80	48.80
10	39.05	16.66	47.52	16.50
25	1.52	0.4	14.44	3.82
40	0.3	0.05	3.60	0.95

Table 9. Maximum PPV values on the blast hole collar and the second mode of discontinuities with different values of decoupling.

Distance from the blast hole (m)	PPV(mm/s)			
	GSI = 75, D = 0		GSI = 50, D = 0	
	DEC = 1/2	DEC = 2/3	DEC = 1/2	DEC = 2/3
0	128.86	105.92	98.98	52.54
10	71.56	30.73	52.04	20.35
25	15.39	5.41	22.46	8.65
40	1.45	0.5	8.94	0.4

Tables 8 and 9 well-demonstrate the effect of using the decoupling technique on reducing the blast damage zone. Accordingly, in the first mode of discontinuities, the development of blast damage zone was lowered by a decrease in coupling (or an increase in decoupling). The damage zone in both models (GSI = 50, D = 0) and (GSI = 75, D = 0), when decoupling equaled 1/2, extended to the location of the first discontinuity. After the collision with the first discontinuity, the wave was substantially weakened, and the passing wave was included within the allowable range (PPV < 50 mm/s), which showed the safe zone of the rock mass. By increasing the decoupling to DEC = 2/3, the damage to the rock mass was diminished, only occurring in the blast hole collar. According to Table 9, the damages to the rock mass were lowered by changing the direction of discontinuities. Therefore, for the DEC = 1/2 in both diorite (GSI = 50, D = 0) and granite (GSI = 75, D = 0), the damages occurred only in the blast hole collar. Meanwhile, the PPV values obtained from the modelings showed that for the DEC = 2/3, it was only the model (GSI = 75, D = 0) in which the damage occurred in the blast hole collar.

The PPV values with the increase in the blast delay time of the holes for both linear and non-linear blasting patterns in the monitoring points are reported in Tables 10-13. For the linear blasting pattern, by comparing Tables 10 and 12, it can be found that by increasing the blast delay time to 100 ms, the damage zone was more in the first mode of discontinuities direction. In this condition the damage zone extended to the location of the second discontinuity (25 m from the blast hole). However, the damage to the rock mass in the model (GSI = 50, D = 0.7) had more development, extending to the location of the third discontinuity (40 m from the blast hole). According to Table 12, in the second mode of discontinuities, the damage to the rock mass was lower, extending to the location of the first discontinuity location. It was only in the model (GSI = 50, D = 0.7) that the development was similar to that of the first mode of discontinuities, extending to 40 m from the blast hole.

Tables 11 and 13 demonstrated that in the non-linear blasting pattern, the damage zone extended more in the first mode of discontinuities compared to the second one. By comparing Tables 10 and 11, it was found that by increasing the blast delay time, the damage to the rock mass was equal in both linear and non-linear blasting patterns. It is revealed that only in the model (GSI = 50, D = 0), the damage zone had more development in the nonlinear blasting pattern compared to the linear one, extending to 25 m from the blast hole.

Table 10. Maximum PPV values on the blast hole collar and the first mode of discontinuities for 100 ms delay time (linear blasting pattern).

Distance from the blast hole (m)	PPV(mm/s)				
	GSI = 75, D = 0	GSI = 75, D = 0.7	GSI = 75, D = 1	GSI = 50, D = 0	GSI = 50, D = 0.7
0	220.37	338.24	333.55	262.74	340.35
10	206.50	201.52	423.90	347.20	492.75
25	60.55	58.35	70.04	123.49	225.70
40	12.61	16.14	22.43	26.66	105.74

Table 11. Maximum PPV values on the blast hole collar and the first mode of discontinuities for 100 ms delay time (nonlinear blasting pattern).

Distance from the blast hole (m)	PPV(mm/s)				
	GSI = 75, D = 0	GSI = 75, D = 0.7	GSI = 75, D = 1	GSI = 50, D = 0	GSI = 50, D = 0.7
0	210.46	270.64	300.22	293.52	337.92
10	217.06	151.56	264.23	215.80	339.18
25	83.97	67.78	69.37	133.83	198.08
40	13.07	17.70	29.10	38.19	109.91

Table 12. Maximum PPV values on the blast hole collar and the second mode of discontinuities for 100 ms delay time (linear blasting pattern).

Distance from the blast hole (m)	PPV(mm/s)				
	GSI = 75, D = 0	GSI = 75, D = 0.7	GSI = 75, D = 1	GSI = 50, D = 0	GSI = 50, D = 0.7
0	200.01	382.91	289.41	205.03	382.76
10	93.71	250.36	293.14	198.81	296.33
25	8.55	24.85	37.46	47.62	155.41
40	0.50	8.48	12.66	18.45	70.71

Table 13. Maximum PPV values on the blast hole collar and the second mode of discontinuities for 100 ms delay time (nonlinear blasting pattern).

Distance from the blast hole (m)	PPV(mm/s)				
	GSI = 75, D = 0	GSI = 75, D = 0.7	GSI = 75, D = 1	GSI = 50, D = 0	GSI = 50, D = 0.7
0	305.52	298.96	261.69	365.78	382.93
10	153.56	197.44	204.31	186.30	210.79
25	13.03	27.15	38.65	87.69	157.28
40	3.86	9.04	13.54	31.93	76.23

5. Conclusions

This study investigated 56 numerical models to determine the effect of changes in four blast design parameters (blast delay time, sub-drilling, decoupling, and blast damage factor, D) on the PPV values in granite and diorite rock masses. The most important results obtained from this work include:

- With an increase in the distance from the blasting location, the wave caused by the blasting of the charge column had a decreasing trend, and the PPV values lowered.

- The results obtained from the numerical modelings demonstrated that the geological discontinuities act as a filter and can reduce the energy of the incident wave. In this regard, the first discontinuity, especially in rocks with higher strength, has the greatest effect on the damping of the blast wave.

- With a reduction in the rock mass strength caused by the increase in the blast damage factor (D), the PPV values in the monitoring points increased.

- The results of this study indicated that by increasing the decoupling (decreasing the coupling), the PPV values could reduce by up to more than 90%, depending on the strength properties and quality of the rock mass. Moreover, it was observed that in the second mode of the discontinuities, the reduction of coupling by 50% and 66.6% in the granite lowered the PPV values at the first discontinuity by 86% and 94%, respectively. The corresponding reductions of PPV values for the diorite were 92.9% and 97.9%, respectively.

- It was concluded that for the first mode of discontinuity as the delay time increased from 0

ms to 100 ms, the PPV values reduced 66.42%. This reduction is 31.3% for the second mode of discontinuities.

- The development of the blast damage zone in the first mode of discontinuities was similar for both linear and non-linear blasting patterns. Meanwhile, for the first mode of discontinuities, the blast damage zone had more development in the linear blasting pattern in the model (GSI = 50, D = 0).

References

[1]. Aloui, M., Bleuzen, Y., Essefi, E., and Abbes, C. (2016). Ground vibrations and air blast effects induced by blasting in open pit mines: Case of Metlaoui Mining Basin, South western Tunisia. Journal of Geology and Geophysics, 5(3).

[2]. Lu, W., Leng, Z., Hu, H., Chen, M., and Wang., G. (2018). Experimental and numerical investigation of the effect of blast-generated free surfaces on blasting vibration. European Journal of Environmental and Civil Engineering, 22(11): 1374-1398.

[3]. Huang, D., Qiu, X., Shi, X., Gou, Y., and Zhou, J. (2019). Experimental and numerical investigation of blast-induced vibration for short-delay cut blasting in underground mining. Shock and Vibration: 2019.

[4]. Bhandari, S., (1997). Engineering rock blasting operations. Balkema.

[5]. Konya, C.J., and Walter, E.J. (1991). Rock blasting and over break control. United States. Federal Highway Administration.

[6]. Hoek, E., and Brown, E.T. (1988). The Hoek-Brown failure criterion- A 1988 update. Proc. 15th Canadian Rock Mechanics Symposium, (Ed. J. H. Curran). Toronto, pp. 31-38.

[7]. Afrasiabian, B., Ahangari, K., and Noorzad, A. (2021). Study on the effect of air deck on ground vibration and development of blast damage zone using 3D discrete element numerical method. Arabian Journal of Geosciences, 14(13): 1-12.

[8]. Chen, Y., Xu, J., Huo, X., and Wang, J. (2019). Numerical simulation of dynamic damage and stability of a bedding rock slope under blasting load. Shock and Vibration: 2019.

[9]. Haghnejad, A., Ahangari, K., Moarefvand, P., and Goshtasbi, K. (2018). Numerical investigation of the impact of geological discontinuities on the propagation of ground vibrations. Geomechanics and Engineering, 14(6): 545-552.

[10]. Haghnejad, A., Ahangari, K., Moarefvand, P., and Goshtasbi, K. (2019). Numerical investigation of the impact of rock mass properties on propagation of ground vibration. Natural Hazards, 96(2): 587-606.

[11]. Kaveh Ahangaran, D., Ahangari, K., and Eftekhari, M. (2022). Numerical analysis of blast-induced damage in rock slopes. Innovative Infrastructure Solutions, 7(1): 1-18.

[12]. Yu, C., Yue, H., Li, H., Zuo, H, Deng, S., and Liu, B. (2019). Study on the attenuation parameters of blasting vibration velocity in jointed rock masses. Bulletin of Engineering Geology and the Environment, 78(7): 5357-5368.

[13]. Liu, Y.Q., Li, H.B., Zhao, J., Li, J.R., and Zhou, Q.C. (2004). UDEC simulation for dynamic response of a rock slope subject to explosions. International Journal of Rock Mechanics and Mining Sciences, 41(SUPPL. 1).

[14]. Hossaini, S.M.F., and Sen, G.C. (2006). A study of the influence of different blasting modes and explosive types on ground vibrations. Iranian Journal of Science & Technology, Transaction B, Engineering, 30, No. B3.

[15]. Torano, J., Rodríguez, R., Diego, I., Rivas, J.M., and Casal, M.D. (2006). FEM models including randomness and its application to the blasting vibrations prediction. Computers and Geotechnics, 33(1): 15-28.

[16]. Xia, X., Li, J., Li, H., Liu, B., Zhou, Q., Zhao, J., and Liu, Y. (2007). Study on damage characteristics of rock mass under blasting load in ling'ao nuclear power station, guangdong province. Chinese Journal of Rock Mechanics and Engineering, 12.

[17]. Zhu, Z. (2009). Numerical prediction of crater blasting and bench blasting. International Journal of Rock Mechanics and Mining Sciences, 6(46): 1088-1096.

[18]. Wie, X.Y., Zhao, Z.Y., and Gu, J. (2009). Numerical simulations of rock mass damage induced by underground explosion. International Journal of Rock Mechanics and Mining Sciences. 46(7): 1206-1213.

[19]. Aliabadian, Z., and Sharafisafa, M. (2014). Numerical modeling of presplitting controlled method in continuum rock masses. Arabian Journal of Geosciences, 7(12): 5005-5020.

[20]. Afrasiabian, B., Ahangari, K., and Noorzad, A. (2021). Study on the effect of air deck on ground vibration and development of blast damage zone using 3D discrete element numerical method. Arabian Journal of Geosciences, 14(13): 1-12.

[21]. Afrasiabian, B., Ahangari, K., and Noorzad, A. (2020). Study on the effects of blast damage factor and blast design parameters on the ground vibration using 3D discrete element method. Innovative Infrastructure Solutions, 5(2): 1-14.

[22]. Mousavi, S.A., Ahangari, K., and Goshtasbi, K. (2022). An Investigation into Bench Health Monitoring under Blast Loading in Hoek-Brown Failure Criterion using Finite Difference Method. Journal of Mining and Environment, 13(3), 875-889.

[23]. Itasca Consulting Group Inc. (2018) 3DEC 5.2, User's guide, Minneapolis.

[24]. Kuhlemeyer, R.L. and Lysmer, J. (1973). Finite element method accuracy for wave propagation problems. Journal of the Soil Mechanics and Foundations Division. 99(SM5): 421–427.

[25]. Hoek, E., and Brown, E.T. (1997). Practical estimates of rock mass strength. International journal of rock mechanics and mining sciences, 34(8): 1165-1186.

[26]. Hoek, E., Carranza-Torres, C.T., and Corkum, B. (2002). Hoek-Brown failure criterion-2002 edition. Proc. the 5th North American rock mechanics symposium. Toronto, pp. 267–73.

[27]. Vlachopoulos, N., and Vazaios, I. (2018). The numerical simulation of hard rocks for tunnelling purposes at great depths: a comparison between the hybrid FDEM method and continuous techniques. Advances in Civil Engineering, 2018.

[28]. Yilmaz, O., and Unlu, T. (2013). Three dimensional numerical rock damage analysis under blasting load. Tunnelling and Underground Space Technology, 38: 266–278.

[29]. Cho, S.H., and Kaneko, K. (2004). Influence of the applied pressure waveform on the dynamic fracture processes in rock. International Journal of Rock Mechanics and Mining Sciences, 41(5): 771-784.

[30]. Duvall, W.I. (1953). Strain-wave shapes in rock near explosions. Geophysics, 18(2): 310-323.

[31]. Jong, Y., Lee, C., Jeon, S., Cho, Y.D., and Shim, D.S. (2005). Numerical modeling of the circular-cut using particle flaw code. Proc. 31st annular conference of explosives and blasting technique, Orlando.

[32]. Starfield, A.M., and Pugliese, J.M. (1968). Compression waves generated in rock by cylindrical explosive charges: a comparison between a computer

model and field measurements. International Journal of Rock Mechanics and Mining Sciences & Geomechanics Abstracts. 5(1): 65-77.

[33]. Ainalis, D., Kaufmann, O., Tshibangu, J.P., Verlinden, O., and Kouroussis, G. (2017). Modelling the source of blasting for the numerical simulation of blast-induced ground vibrations: a review. Rock mechanics and rock engineering. 50(1): 171-193.

[34]. Bhasin, R., and Kaynia, A.M. (2004). Static and dynamic simulation of a 700-m high rock slope in western Norway. Engineering Geology, 71(3): 213-226.

[35]. Leidig, M., Bonner, J.L., Rath, T., and Murray, D. (2010). Quantification of ground vibration differences from well-confined single-hole explosions with variable velocity of detonation. International Journal of Rock Mechanics and Mining Sciences, 47(1): 42-49.

[36]. Sainoki, A., and Mitri, H.S. (2014). Dynamic behavior of mining-induced fault slip. International Journal of Rock Mechanics and Mining Sciences, 66: 19-29.

[37]. Kuili, S., and Sastry, V.R. (2018). A numerical modelling approach to assess the behaviour of underground cavern subjected to blast loads. International Journal of Mining Science and Technology, 28(6): 975-983.

[38]. Kumar, R., Choudhury, D., and Bhargava, K. (2016). Determination of blast-induced ground vibration equations for rocks using mechanical and geological properties. Journal of Rock Mechanics and Geotechnical Engineering, 8(3): 341-349.

[39]. Nguyen, H., Bui, X.N., and Moayedi, H. (2019). A comparison of advanced computational models and experimental techniques in predicting blast-induced ground vibration in open-pit coal mine. Acta Geophysica, 67(4): 1025-1037.

[40]. Hoek E. (2012). Blast damage factor D. Technical Note for Rocscience.

[41]. Hustrulid, W.A. (1999). Blasting principles for open pit mining: general design concepts. Balkema, Rotterdam.

[42]. Hustrulid, W.A., Kuchta, M., and Martin, R.K. (2013). Open pit mine planning and design, two volume set & CD-ROM pack. CRC Press.

[43]. Singh, P., and Narendrula, R. (2007). The influence of rock mass quality in controlled blasting. Proc. 26th international conference on ground control in mining, Morgantown, pp. 314-331.

[44]. Taqieddin, S.A. (1986). Ground vibration levels: prediction and parameters. Mining Science and Technology, 3(2): 111-115.

[45]. Leidig, M., Bonner, J.L., Rath, T., and Murray, D. (2010). Quantification of ground vibration differences from well-confined single-hole explosions with variable velocity of detonation. International Journal of Rock Mechanics and Mining Sciences, 47(1): 42-49.

[46]. Matidza, M.I., Jianhua, Z., Gang, H., and Mwangi, A.D. (2020). Assessment of blast-induced ground vibration at jinduicheng molybdenum open pit mine. Natural Resources Research, 2020: 1-11.

[47]. Xu, J., Kang, Y., Wang, X., Feng, G., and Wang, Z. (2019). Dynamic characteristics and safety criterion of deep rock mine opening under blast loading. International Journal of Rock Mechanics and Mining Sciences, 119: 156-167.

[48]. Silva J, Worsey T, and Lusk B. (2019). Practical assessment of rock damage due to blasting. International Journal of Mining Science and Technology, 29(3): 379-385.

[49]. Langefors, U., and Kihlström, B. (1978). The modern technique of rock blasting. Wiley, New York.

[50]. Nicholls, H.R., Johnson, C.F., and Duvall, W.I. (1971). Blasting vibration effects on structures. US Bureau of Mines report of investigation 656.

[51]. Oriard, L.L. (1970). Dynamic effects on rock masses from blasting operations. Woodward-Clyde & Associates.

ارزیابی اثرات پارامترهای فاکتور آسیب انفجار، اضافه حفاری، دکوپلینگ و زمان تاخیر بین چال‌های انفجاری بر حداکثر سرعت ذرات با استفاده از مدل‌سازی عددی

بیژن افراسیابیان[1]، کاوه آهنگری[1]*، و علی نورزاد[2]

1- بخش مهندسی معدن، دانشگاه علوم تحقیقات، تهران، ایران
2- دانشکده مهندسی عمران، آب و محیط زیست، دانشگاه شهید بهشتی، تهران، ایران

چکیده:

سطوح بالای ارتعا شات نا شی از عملیات انفجار در معادن روباز می‌تواند اثرات نامطلوبی مانند تخریب سازه‌های سطحی پیرامونی را ایجاد کند. بنابراین شناسایی عوامل موثر در کاهش اثرات مخرب ارتعا شات زمین در معادن روباز و پایش آنها ضروری ا ست. این مطالعه به برر سی اثرات برخی از مهم‌ترین پارامترهای طراحی انفجار در یک ردیف از چال‌های انفجاری می‌پردازد. با توجه به مزایای روش‌های عددی، از روش المان گسسته سه بعدی برای این منظور استفاده می‌شود. مقادیر حداکثر سرعت ذرات (PPV) در امتداد چال مرکزی در فواصل یک متری اندازه‌گیری می‌شود. نتایج به‌دست آمده نشان می‌دهد که افزایش فاکتور آسیب انفجار و زمان تأخیر بین چال‌های انفجار منجر به ارائه مقادیر بالاتر PPV می‌شود. با این حال، افزایش زمان تاخیر تاثیر قابل توجهی در کاهش توسعه منطقه آسیب انفجار ندارد. از سوی دیگر، با افزایش دکوپلینگ، مقادیر PPV کاهش می‌یابد که منجر به کاهش قابل توجهی در ارتعاش زمین و آ سیب توده سنگ می شود. همچنین مشاهده گردید که حذف اضافه حفاری، ارتعا شات زمین را به میزان قابل توجهی کاهش نمی‌دهد. تحلیل نتایج بدست آمده از مدل‌سازی عددی نشان می‌دهد که ناپیوستگی‌های توده سنگ به عنوان یک فیلتر عمل می‌کند که می‌تواند انرژی موج را تا بیش از 90 درصد کاهش دهد. علاوه بر این، مشخص شد که جهت ناپیوستگی‌ها نیز بر انتشار امواج ناشی از انفجار تأثیر می‌گذارد. در شرایطی که ناپیوستگی‌ها مخالف سطح شیب باشند، مقادیر PPV کاهش یافته و ناحیه آسیب دیده کمتر توسعه می‌یابد.

کلمات کلیدی: حداکثر سرعت ذرات، آسیب، ناپیوستگی‌ها، فشار چال انفجاری، مدل‌سازی عددی.